# Observation of Fano line shapes arising from coupling between surface plasmon polariton and waveguide modes

Hayashi, Shinji

Nesterenko, D. V.

Rahmouni, A.

Sekkat, Z.

(Citation)
Applied Physics Letters,108(5):051101-051101

(Issue Date)
2016-02-01

(Resource Type)
journal article

(Version)
Version of Record

AIP Applied Physics Letters

# Observation of Fano line shapes arising from coupling between surface plasmon polariton and waveguide modes

S. Hayashi, D. V. Nesterenko, A. Rahmouni, and Z. Sekkat

Citation: Applied Physics Letters **108**, 051101 (2016); doi: 10.1063/1.4940984
View online: http://dx.doi.org/10.1063/1.4940984
View Table of Contents: http://scitation.aip.org/content/aip/journal/apl/108/5?ver=pdfcov
Published by the AIP Publishing



# Observation of Fano line shapes arising from coupling between surface plasmon polariton and waveguide modes

S. Hayashi,[1,2,a)] D. V. Nesterenko,[2] A. Rahmouni,[2] and Z. Sekkat[2,3,4]
[1]*Department of Electrical and Electronic Engineering, Graduate School of Engineering, Kobe University, Kobe 657-8501, Japan*
[2]*Optics and Photonics Center, Moroccan Foundation for Science, Innovation and Research (MAScIR), Rabat 10100, Morocco*
[3]*Faculty of Sciences, University Mohamed V, Rabat 10010, Morocco*
[4]*Graduate School of Engineering, Osaka University, Osaka 585-0871, Japan*

(Received 17 December 2015; accepted 18 January 2016; published online 1 February 2016)

We demonstrate experimentally the generation of narrow Fano line shapes in planar multilayer structures. The Fano line shape originates from coupling between a high loss surface plasmon polariton mode with a low loss planar waveguide mode. The line shape is shown to depend strongly on the structural parameters that govern the position of the waveguide mode and the coupling strength, and to be in good agreement with results of electromagnetic calculations. © *2016 AIP Publishing LLC*. [http://dx.doi.org/10.1063/1.4940984]

The interaction between electromagnetic (EM) modes supported by nanostructures plays a crucial role in determining their optical properties. It is well known that the asymmetric line shapes, so-called Fano line shapes, are generated in the optical response, when dark modes with sharp resonances interact with bright modes with broad resonances.[1–4] Although the Fano line shape has initially been observed in the atomic spectra and interpreted quantum mechanically by Fano as due to the interference of a discrete quantum level with a continuum state,[1,5] the analogous line shapes are observed in a variety of physical systems and can even be described by a model of classical two coupled harmonic oscillators.[6,7] In recent years, great efforts have been made to generate Fano line shapes in plasmonic nanostructures and apply them to develop novel optical devices such as optical sensors and switches.[2] To date, a variety of plasmonic nanostructures, including metallic nanowire arrays,[8] clusters of nanoparticles,[9–13] disk/ring nanocavities,[14–16] and metal-insulator-metal waveguides coupled to resonators,[17] are known to exhibit Fano line shapes. In spite of the intensive work done, the fabrication of the nanostructures is not always easy and is time consuming, preventing their real applications. Furthermore, the underlying physics that generates the Fano resonances is not always well understood.

In this letter, we report on the experimental observation of the Fano line shapes in planar multilayer systems. The structures studied are simple and do not require the use of nanofabrication techniques. Our planar structure allows coupling between a surface plasmon polariton (SPP) at a metal-dielectric interface and a planar waveguide (PWG) mode supported by a stack of dielectric layers. We show that sharp Fano line shapes appear in the attenuated total reflection (ATR) spectra when the structural parameters are appropriately chosen. The experimental results agree fairly well with the results of the EM calculations, and the physical origin of the appearance of the Fano line shapes is unambiguously identified by the coupling between the SPP and PWG modes.

The structure of the samples prepared is shown schematically in Fig. 1(a). As can be seen from Fig. 1(b), this structure can be regarded as a combination of a metal-dielectric interface that supports SPP modes and a stack of three dielectrics that supports PWG modes. To prepare the samples, a Ag film of approximately 45 nm in thickness was deposited on a cleaned SF10 glass substrate by a vacuum evaporation technique. A fluoropolymer Cytop film was then spin coated on the Ag film; Cytop solution of ∼6 wt. % was used. To complete the sample, a poly(methyl methacrylate) (PMMA) film was spin coated on top of the Cytop film from toluene solution with a PMMA concentration of ∼7 wt. %. The thickness of the Ag film was monitored by a quartz microbalance during the deposition. The thicknesses of the Cytop and PMMA films were controlled by choosing appropriate rotation speeds of spin coating. The thicknesses and dielectric constants of the films were estimated by fitting theoretical ATR spectra with the experimental ones (*vide infra*). Since the prepared multilayer samples allow the coupling

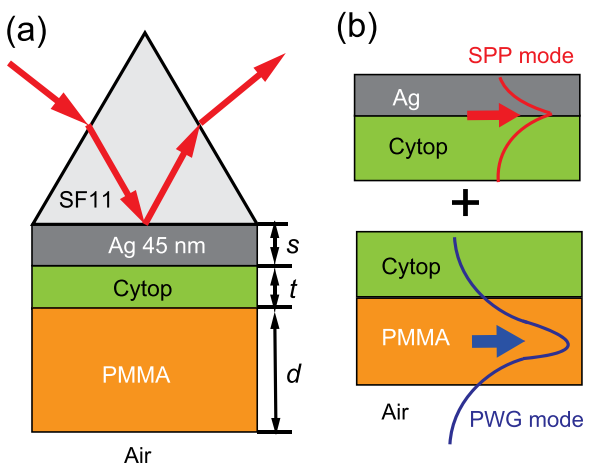


FIG. 1. (a) Structure of samples prepared. (b) Metal-dielectric interface that supports SPP modes and stack of dielectrics that supports PWG modes.

[a)]s.hayashi@dragon.kobe-u.ac.jp

 

between the SPP and PWG modes, hereafter we call the samples as SPP-PWG hybrid samples. For comparison purposes, we also prepared metal-clad waveguide (MCWG) samples, which have only the PMMA film directly deposited on the Ag film.

The optical setup used to measure the ATR spectra in a Kretschmann configuration is similar to that described in detail in our previous paper (Fig. 2 in Ref. 18). The multilayer sample was pasted onto the bottom surface of a 60°-prism made of an SF11 glass with the aid of index matching oil. The prism with the sample was mounted on a computer-controlled rotating stage. For the measurements of $\theta$-scan ATR spectra, $p$-polarized light from a He-Ne laser with a wavelength of 632.8 nm was incident on the prism through a chopper. The intensity of the reflected light was measured as a function of the angle of incidence, $\theta$, using a Si photodiode connected to a lock-in-amplifier. The reflectance spectra were obtained by normalizing the intensity data recorded with the sample to that recorded for a bare part of the prism. The precision of the incident angle (internal angle inside the prism) in the present measurements is around 0.018°.

We first present, in Fig. 2(a), a typical $\theta$-scan ATR spectrum obtained for an MCWG sample with a PMMA waveguide. For this sample, the PMMA film was spin coated with a speed of 3000 rpm. The ATR dip appearing around 65° is due to the excitation of SPP at the Ag/PMMA interface and those appearing at lower angles are due to the excitation of the PWG modes assigned to the 0th- and 1st-order transverse magnetic (TM) modes, denoted as $TM_0$ and $TM_1$, respectively. The fluctuation in the reflectance seen around 60° is caused by the interference of light beams multiply reflected inside the 60°-prism.

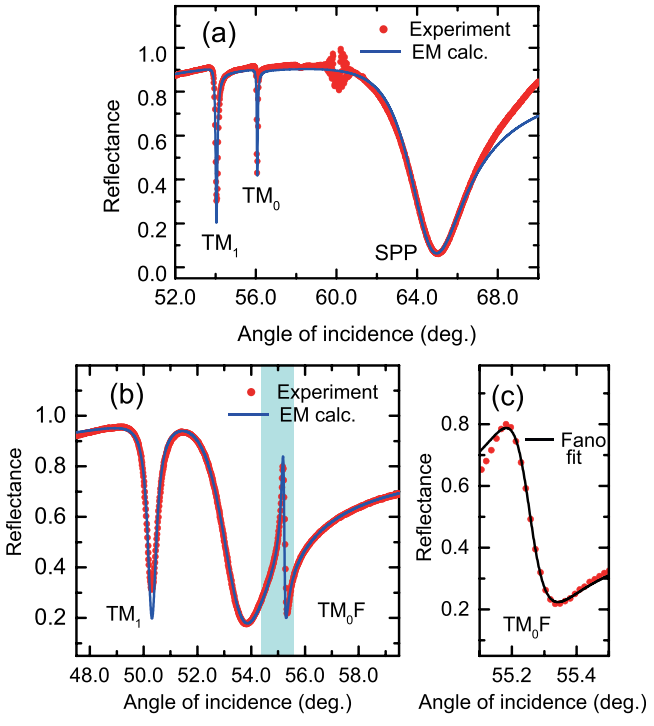


FIG. 2. (a) Experimental (dots) and theoretical (solid curve) ATR spectra of an MCWG sample with an PMMA film spin coated with 3000 rpm (estimated thickness of $d = 1790$ nm). (b) Experimental (dots) and theoretical (solid curve) ATR spectra of an SPP-PWG hybrid sample with a Cytop film spin coated with 3000 rpm (estimated thickness of $t = 400$ nm) and an PMMA film spin coated with 7000 rpm (estimated thickness of $d = 920$ nm). (c) Fit of the asymmetric line shape to the Fano line shape function.

We attempted to reproduce theoretically the experimental spectrum by the EM calculation. We used a $2 \times 2$ transfer matrix method.[19,20] We assumed a multilayer stack consisting of an SF11 glass, a Ag layer, a PMMA layer, and air. In the calculation, we omitted the SF10 substrate used in the experiments. When the SF10 substrate is inserted between the SF11 glass and the Ag layer in the calculation, small fluctuations appear in the theoretical spectra; the fluctuations originate from the interference of light caused by the multiple reflections inside the SF10 substrate. However, such fluctuations are smeared out and not observed in the experiments. As demonstrated below, the present experimental results can be well reproduced without the SF10 substrate. A value of the dielectric constant of SF11 at $\lambda = 632.8$ nm, $\varepsilon_p = 3.1634$, was taken from a database.[21] We searched for the values of thickness and dielectric constant of the Ag and PMMA layers that reproduce well the experimental spectrum. The solid curve in Fig. 2(a) is a theoretical spectrum generated by a set of parameters: $s = 48$ nm and $\varepsilon_{Ag} = -14.9493 + i1.6789$ for the Ag layer, and $d = 1790$ nm and $\varepsilon_{PMMA} = 2.2136 + i8.9268 \times 10^{-4}$ for the PMMA layer. The overall fit of the calculated spectrum to the experimental points is quite good except for the large-angle region of $\theta > 67°$. An estimate of the PMMA thickness obtained from this fitting procedure is thus $d = 1790$ nm. The above values of the dielectric constants are close to the literature values,[21] even though the optical constants of thin films vary considerably depending on the method and condition of preparation. The spectrum presented in Fig. 2(a) is typical of the MCWG structure which is in good agreement with the previously reported spectra.[22,23] It should be stressed here that, in the MCWG structure, the in-plane wavenumbers of the SPP and PWG modes do not coincide, and consequently, the interaction between them is impossible.

In Fig. 2(b), an ATR spectrum obtained for an SPP-PWG hybrid sample with a Cytop intermediate layer is shown. For this sample, the Cytop and PMMA films were prepared with rotation speeds of 3000 and 7000 rpm, respectively. We see that the presence of the intermediate Cytop layer greatly modifies the ATR spectrum. The broad ATR dip corresponding to the SPP excitation is shifted to an angle (~55°) lower than that for the MCWG sample (~65°, Fig. 2(a)). This is because the in-plane wavenumber of the SPP mode at the Ag/Cytop interface is smaller than that at the Ag/PMMA interface, reflecting a smaller value of the real part of the dielectric constant of Cytop (1.796 according to Ref. 24) relative to that of the PMMA (~2.214 according to our estimate). In the SPP-PWG hybrid sample prepared, the $TM_0$ PWG mode is tuned into the broad SPP dip. A salient feature in the observed spectrum is the appearance of a very narrow asymmetric line shape around 55° denoted as $TM_0F$. We also see a dip corresponding to the $TM_1$ PWG mode at 50.32°. We calculated the theoretical spectra adding a Cytop layer in between the Ag and PMMA layers. The solid curve shown in Fig. 2(b) is a theoretical fit obtained by a set of parameters: $s = 45$ nm and $\varepsilon_{Ag} = -15.5075 + i3.1010$ for the Ag layer; $t = 400$ nm and $\varepsilon_{Cytop} = 1.8117 + i2.6900 \times 10^{-3}$ for the Cytop layer; and $d = 920$ nm and $\varepsilon_{PMMA} = 2.2141 + i2.9760 \times 10^{-4}$ for the PMMA layer. Figure 2(b) demonstrates that the experimental

spectrum of the SPP-PWG hybrid sample exhibiting the asymmetric line shape can be reproduced fairly well by the EM calculation.

We checked whether the observed asymmetric line shape can fit to a Fano line shape function. We used the following function, which was slightly modified from its initial form,[2] to take into account the nonzero value of the reflectance minimum and the scale factor:

$$R(\theta) = R_0 + S\frac{(F\gamma + \theta_0 - \theta)^2}{(\theta_0 - \theta)^2 + \gamma^2}, \quad (1)$$

where $\theta_0$ and $\gamma$ denote the position and width of the Fano resonance, respectively; $F$ is the so-called Fano factor, which describes the degree of the asymmetry in the line shape; $R_0$ and $S$ are the minimum value of the reflectance and the scale factor, respectively. In Fig. 2(c), the experimental points around the resonance and the best fit curve are compared. The best fit curve was obtained by a set of parameters: $\theta_0 = 55.24998^\circ$, $\gamma = 0.07913^\circ$, $F = 1.1683$, $R_0 = 0.22422$, and $S = 0.23826$. The overall good fit obtained allows us to conclude that the presently observed asymmetric line shape is indeed of the Fano type. The slight deviation of the experimental points away from the resonance angle at the low-angle side is due to the fact that the variation of the reflectance in the SPP dip around the Fano resonance is relatively rapid, while a flat continuum is assumed in the derivation of the Fano line shape function.[1,2] A quality factor calculated by $Q = \theta_0/2\gamma$ with the above fitting parameters is as large as ~350. This value is more than one order of magnitude larger than Q factors of ~10 reported in early studies of the Fano resonance in plasmonic nanostructures.[2] Moreover, the present Q factor is even larger than those of ~100 recently achieved experimentally in plasmonic nanostructures.[25,26]

The Fano resonances observed in plasmonic nanostructures have commonly been interpreted in terms of coupling between the bright mode characterized by a broad resonance and the dark mode characterized by a sharp resonance.[2–4] In the present multilayer structure, the SPP mode at the Ag/Cytop interface is regarded as a bright mode with a broad resonance and the $TM_0$ PWG mode in the Cytop/PMMA/Air waveguide structure is regarded as a dark mode with a sharp resonance. The two modes can interact with each other through the overlap of their evanescent electromagnetic fields inside the intermediate Cytop layer.[27] When the PMMA thickness is appropriately chosen, the PWG mode can be tuned into the broad SPP resonance. An appropriate choice of the Cytop thickness results in a well-defined Fano line shape as experimentally demonstrated above. The present SPP-PWG hybrid structure is purely an EM system, whose optical response is described by the EM theory based on the Maxwell's equations. However, as discussed in detail in our previous theoretical paper,[28] an almost perfect analogy holds between the present EM system and the mechanical system of two coupled harmonic oscillators. The physics underlying the present EM system and the coupled-oscillator system is the same, confirming that the Fano resonance presently observed is due to the coupling between the SPP and PWG modes.

In the present multilayer samples, the position of the PWG modes is controlled by the PMMA thickness $d$, and the strength of the coupling between the PWG and SPP modes is controlled by the Cytop thickness $t$. To produce a well-defined Fano line shape, $d$ and $t$ have to be adjusted appropriately. To study the influence of $d$ and $t$ on the Fano line shape, we prepared various samples with different $d$ and $t$. The results obtained by varying $d$ while fixing $t$ are presented in Figs. 3(a)–3(c). Those obtained by varying $t$ while fixing $d$ are given in Figs. 3(d)–3(f). The experimental and theoretical spectra shown in Figs. 3(b) and 3(d) are identical to those shown in Fig. 2(b). The rotation speeds of spin coating used are indicated in the figures.

The experimental ATR spectra shown in Figs. 3(a)–3(c) demonstrate clearly that the Fano resonance shifts to lower angles, as $d$ decreases. The dip corresponding to the $TM_1$ PWG mode also shifts to lower angles. In Fig. 3(c), the sharp resonance is located near the middle of the broad dip; the line shape approaches that of so-called electromagnetically induced transparency (EIT)[6,29,30] or plasmon-induced transparency (PIT),[31] which is characterized by a sharp hole at the middle of a broad resonance band. In Figs. 3(a)–3(c), calculated ATR spectra are also presented. To obtain the spectra, the parameters of the Cytop layer were fixed at the same values as those used to reproduce the experimental spectrum shown in Fig. 2(b), while the parameters of the Ag and PMMA layers were so adjusted to well reproduce the experimental spectra. The spectrum shown in Fig. 3(a) was obtained by a set of the parameters: $s = 47$ nm and $\varepsilon_{Ag} = -17.0153 + i1.1705$ for the Ag layer, $d = 1050$ nm and $\varepsilon_{PMMA} = 2.21712 + i5.9560 \times 10^{-4}$ for the PMMA layer. The spectrum shown in Fig. 3(c) was obtained by a set of the parameters: $s = 47$ nm and $\varepsilon_{Ag} = -15.0099 + i2.6666$ for the Ag layer, $d = 803$ nm and $\varepsilon_{PMMA} = 2.2082 + i2.9720 \times 10^{-4}$ for the PMMA layer. We see that the dependence of the spectrum on $d$ is very well reproduced by the EM calculations. The physical origin of the shift of the Fano resonance is the change in the in-plane wavenumber of the $TM_0$ PWG mode; the wavenumber decreases as $d$ decreases, letting the corresponding Fano resonance appear at lower angles. The same argument applies to the shift of the $TM_1$ dip.

The experimental spectra shown in Figs. 3(d)–3(f) demonstrate that the Fano resonance broadens and splits into two dips as $t$ decreases. As $t$ decreases, the $TM_1$ dip shifts to lower angles. Theoretical spectra shown in the figures were obtained by fixing the parameters of the PMMA layer at the values used to reproduce the spectrum of Fig. 2(b). Other parameters used for the theoretical spectrum in Fig. 3(e) are $s = 46$ nm and $\varepsilon_{Ag} = -14.7326 + i3.3278$ for the Ag layer, and $t = 285$ nm and $\varepsilon_{Cytop} = 1.8306 + i2.7100 \times 10^{-3}$ for the Cytop layer. Those for the spectrum in Fig. 3(f) are $s = 47$ nm and $\varepsilon_{Ag} = -14.0465 + i4.0802$ for the Ag layer, and $t = 178$ nm and $\varepsilon_{Cytop} = 1.7849 + i2.6700 \times 10^{-4}$ for the Cytop layer.

We see again that the overall dependence of the spectrum on $t$ is reproduced very well by the EM calculations. The broadening and splitting of the resonance can be explained in terms of the increase in the strength of coupling between the SPP and PWG modes. As predicted by the mechanical model of two coupled oscillators and confirmed by

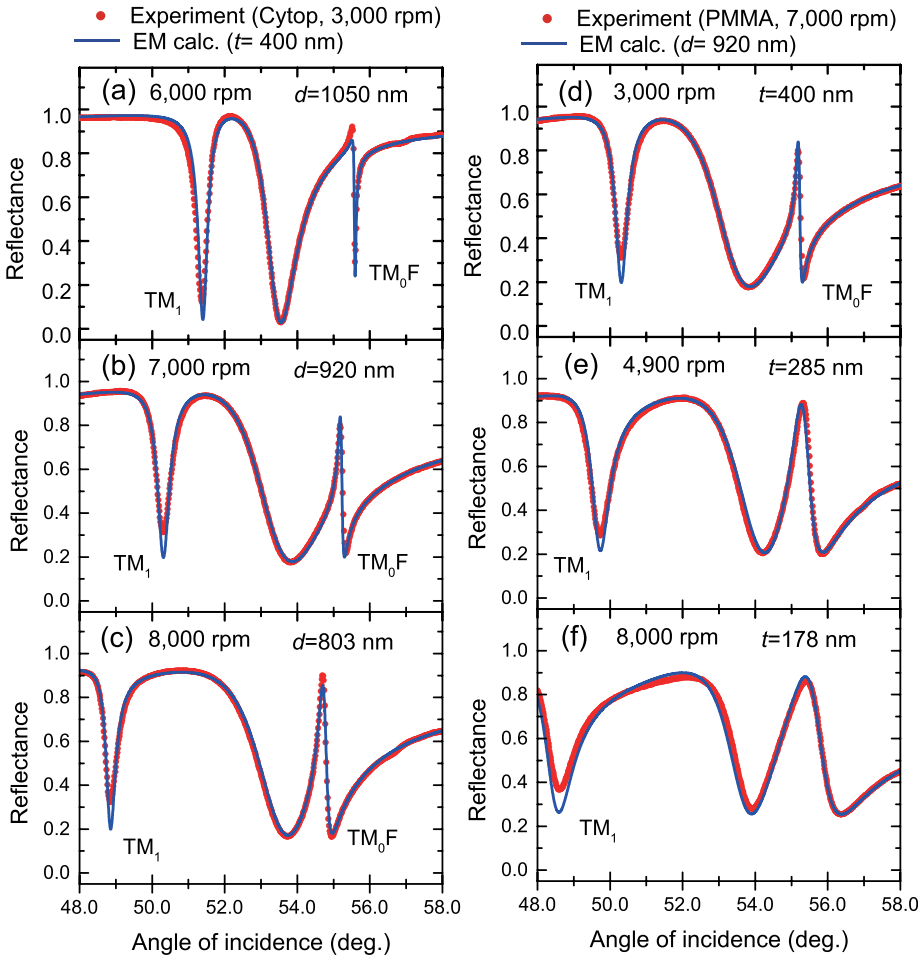


FIG. 3. (a)–(c) Dependence of experimental (dots) and theoretical (solid curve) ATR spectrum on $d$. (d)–(f) Dependence of experimental (dots) and theoretical (solid curve) ATR spectrum on $t$. For the $d$-dependence, the samples were prepared fixing the speed of Cytop coating at 3000 rpm, while setting that of PMMA coating at 6000 rpm (a), 7000 rpm (b), and 8000 rpm (c), respectively. For the $t$-dependence, the samples were prepared fixing the speed of PMMA coating at 7000 rpm, while setting that of Cytop coating at 3000 rpm (d), 4900 rpm (e), and 8000 rpm (f), respectively. The Cytop and PMMA thicknesses estimated from the theoretical fits are given in the figures.

the EM calculation,[28] sharp Fano resonances appear when the coupling is sufficiently weak. In strong coupling cases, the hybridization of the interacting modes results in well separated hybrid modes, generating line shapes that are better described by a superposition of two independent resonances rather than the Fano resonance.[32–34] The line shape changes continuously depending on the coupling strength and it is difficult to precisely set the boundary between the weak and strong coupling cases. However, the line shape seen around 55° in Fig. 3(f) is better described as the superposition of two reflectance dips, which is the manifestation of the strong coupling case.

The SPP-PWG hybrid structure can be used as a sensor in exactly the same way as the conventional surface plasmon resonance (SPR) sensor. In the case of bulk sensing, a sensing medium such as water is placed on top of the waveguide layer and the change in the refractive index of the sensing medium is detected by monitoring either the shift of the ATR resonance curve or the change in the intensity of the reflected light at a fixed angle of incidence. In the latter case, the sensitivity by intensity is defined by the partial derivative of the reflectance with respect to the refractive index, $\partial R/\partial n$, and its maximum value gives the figure of merit $\mathrm{FOM_I}$.[35] According to our previous simulations made for an SPP-PWG hybrid structure consisting of a SF10 prism, Au, Cytop, and ZnS-$SiO_2$ layers surrounded by water, the steep part of the Fano resonance curve in an optimized structure leads to an $\mathrm{FOM_I}$ value $\sim 10^3$ times larger than that of the conventional SPR sensor with a single Au layer.[27,28] The large $\mathrm{FOM_I}$ value stems from the steepness of the high-Q Fano resonance. Our recent calculations (to be published elsewhere[36]) demonstrate that the replacement of the ZnS-$SiO_2$ waveguide layer by a PMMA layer can further enhance the $\mathrm{FOM_I}$ up to a factor of $\sim 10^5$ relative to the conventional SPR sensor. It is also possible to apply the present structure to surface-enhanced spectroscopies, such as the surface-enhanced Raman and fluorescence spectroscopy. At the Fano resonance, highly enhanced electric fields are generated at the waveguide surface and can enhance the spectroscopic signals of molecules adsorbed on the surface. The field enhancement factor recently estimated for the optimized structure with the PMMA waveguide is as large as $\sim 10^7$ (to be published elsewhere[36]). A great advantage of using the SPP-PWG hybrid structure in the enhanced fluorescence spectroscopy is the suppression of fluorescence quenching caused by the energy transfer from excited molecules to the metal. In the structure, the distance between the metal and molecules is large enough to avoid the energy transfer.

In conclusion, we have demonstrated the feasibility of observing narrow Fano line shapes in planar multilayer structures. The Fano line shape arises from the coupling between the SPP and PWG modes and was shown to depend strongly on the structure parameters. The experimental results are in good agreement with the results of the EM calculation. Our results may open a new avenue for realizing sensors with extremely high sensitivities and enhanced spectroscopies with extremely high enhancement factors.

This work was supported by an Osaka University International Joint Research Promotion Program: The Handai project.

[1]A. E. Miroshnichenko, S. Flach, and Y. S. Kivshar, Rev. Mod. Phys. **82**, 2257 (2010).
[2]B. Luk'yanchuk, N. I. Zheludev, S. A. Maier, N. J. Halas, P. Nordlander, H. Giessen, and C. T. Chong, Nat. Mater. **9**, 707 (2010).
[3]B. Gallinet and O. J. F. Martin, ACS Nano **5**, 8999 (2011).
[4]Y. Francescato, V. Giannini, and S. A. Maier, ACS Nano **6**, 1830 (2012).
[5]U. Fano, Phys. Rev. **124**, 1866 (1961).
[6]G. L. Garrido Alzar, M. A. G. Martinez, and P. Nussenzveig, Am. J. Phys. **70**, 37 (2002).
[7]Y. S. Joe, A. M. Satanin, and C. S. Kim, Phys. Scr. **74**, 259 (2006).
[8]A. Christ, Y. Ekinci, H. H. Solak, N. A. Gippus, S. G. Tichodeev, and O. J. F. Martin, Phys. Rev. B **76**, 201405(R) (2007).
[9]J. B. Lassister, H. Sobhani, J. A. Fan, J. Kundu, F. Capasso, P. Nordlander, and N. J. Halas, Nano Lett. **10**, 3184 (2010).
[10]J. B. Lassister, H. Sobhani, M. W. M. W. S. Knight, P. Nordlander, and N. J. Halas, Nano Lett. **12**, 1058 (2012).
[11]S. N. Sheikholeslami, A. Garcia-Extarri, and J. A. Dionne, Nano Lett. **11**, 3927 (2011).
[12]W.-S. Chang, J. B. Lassister, P. Swanglap, H. Sobhani, S. Khatua, P. Nordlander, N. J. Halas, and S. Link, Nano Lett. **12**, 4977 (2012).
[13]Z.-J. Yang, Q.-Q. Wang, and H.-Q. Lin, Appl. Phys. Lett. **103**, 111115 (2013).
[14]Y. Sonnerfraud, N. Verellen, H. Sobhani, G. A. E. Vandenbosch, V. V. Moshchalkov, P. V. Dorpe, P. Nordlander, and S. A. Maier, ASC Nano **4**, 1664 (2010).
[15]Y. H. Fu, J. B. Zhang, Y. F. Yu, and B. Luk'yanchuk, ACS Nano **6**, 5130 (2012).
[16]J. Li, T. Liu, H. Zheng, J. Dong, E. He, W. Gao, Q. Han, C. Wang, and Y. Wu, Plasmonics **9**, 1439 (2014).
[17]J. Qi, C. Z., J. Chen, Y. Li, W. Qiang, J. Xu, and Q. Sun, Opt. Express **22**, 14688 (2014).
[18]S. Rehman, A. Rahmouni, T. Mahfoud, D. V. Nesterenko, and Z. Sekkat, Plasmonics **9**, 381 (2014).
[19]C. E. Reed, J. Giergiel, J. C. Hemminger, and S. Ushioda, Phys. Rev. B **36**, 4990 (1987).
[20]C. C. Katsidis and D. I. Siapkas, Appl. Opt. **41**, 3978 (2002).
[21]M. N. Polyanskiy, see http://refractivindex.info/ for Refractive index database (2015).
[22]Z. Salamon, H. A. Macleod, and G. Tollin, Biophys. J. **73**, 2791 (1997).
[23]W. Knoll, Annu. Rev. Phys. Chem. **49**, 569 (1998).
[24]J. Dostalek, A. Kasry, and W. Knoll, Plasmonics **2**, 97 (2007).
[25]W. Cao, R. Singh, I. A. I. Al-Naib, M. He, A. J. Taylor, and W. Zhang, Opt. Lett. **37**, 3366 (2012).
[26]P. Gu, M. Wan, Q. Shen, X. He, Z. Chen, P. Zhan, and Z. Wang, Appl. Phys. Lett. **107**, 141908 (2015).
[27]S. Hayashi, D. V. Nesterenko, and Z. Sekkat, Appl. Phys. Express **8**, 022201 (2015).
[28]S. Hayashi, D. V. Nesterenko, and Z. Sekkat, J. Phys. D: Appl. Phys. **48**, 325303 (2015).
[29]S. E. Harris, Phys. Today **50**(7), 36 (1997).
[30]M. Fleischhauer, A. Imamonglu, and J. P. Marangos, Rev. Mod. Phys. **77**, 633 (2005).
[31]S. Zhang, D. A. Genov, Y. Wang, M. Liu, and X. Zhang, Phys. Rev. Lett. **101**, 047401 (2008).
[32]J. Bellesa, C. Bonnand, J. C. Plenet, and J. Mugnier, Phys. Rev. Lett. **93**, 036404 (2004).
[33]N. J. Halas, S. Lal, W.-S. Chang, S. Link, and P. Nordlander, Chem. Rev. **111**, 3913 (2011).
[34]S. Hayashi, Y. Ishigaki, and M. Fujii, Phys. Rev. **86**, 045408 (2012).
[35]D. V. Nesterenko and Z. Sekkat, Plasmonics **8**, 1585 (2013).
[36]D. V. Nesterenko, S. Hayashi, and Z. Sekkat, "Extremely narrow resonances, giant sensitivity and field enhancement in low-loss waveguide sensors," J. Opt. (submitted).